Augmenting osteoporotic bone regeneration through a hydrogel-based rejuvenating microenvironment

Xiaoting Zhang [a,b,c,1], Boguang Yang [b,1], Lu Feng [a,b,c], Xiayi Xu [g], Chenmin Wang [h], Yuk-wai Lee [d,e,f], Ming Wang [a,b,c], Xuan Lu [a,b,c], Ling Qin [a,b], Sien Lin [a,b,c,**], Liming Bian [g,***], Gang Li [a,b,c,*]

[a] *Musculoskeletal Research Laboratory, Department of Orthopaedics & Traumatology, The Chinese University of Hong Kong, Prince of Wales Hospital, Hong Kong, China*
[b] *Stem Cells and Regenerative Medicine Laboratory, Li Ka Shing Institute of Health Sciences, The Chinese University of Hong Kong, Prince of Wales Hospital, Hong Kong, China*
[c] *The CUHK-ACC Space Medicine Centre on Health Maintenance of Musculoskeletal System, The Chinese University of Hong Kong Shenzhen Research Institute, Shenzhen, PR China*
[d] *SH Ho Scoliosis Research Laboratory, Department of Orthopaedics and Traumatology, The Chinese University of Hong Kong, Hong Kong, China*
[e] *Joint Scoliosis Research Center of the Chinese University of Hong Kong and Nanjing University, The Chinese University of Hong Kong, Hong Kong, China*
[f] *Li Ka Shing Institute of Health Sciences, The Chinese University of Hong Kong, China*
[g] *School of Biomedical Sciences and Engineering, Guangzhou International Campus, South China University of Technology, Guangzhou, 511442, PR China*
[h] *Department of Orthopaedics and Traumatology, The University of Hong Kong, Hong Kong, China*

ARTICLE INFO

ABSTRACT

Osteoporotic bone defects pose a significant challenge for bone regeneration as they exhibit impaired healing capacity and delayed healing period. To address this issue, this study introduces a hydrogel that creates a rejuvenating microenvironment, thereby facilitating efficient bone repair during the initial two weeks following bone defect surgery. The hydrogel, named GelHFS, was created through host-guest polymerization of gelatin and acrylated β-cyclodextrin. Incorporation of the human fetal mesenchymal stem cell secretome (HFS) formed GelHFS hydrogel aimed at mimicking a rejuvenated stem cell niche. Our results demonstrated that GelHFS hydrogel promotes cell stellate spreading and osteogenic differentiation via integrin β1-induced focal adhesion pathway. Implantation of GelHFS hydrogel in an osteoporotic bone defect rat model recruited endogenous integrin β1-expressing cells and enhanced new bone formation and bone strength. Our findings reveal that GelHFS hydrogel provides a rejuvenating niche for endogenous MSCs and enhances bone regeneration in osteoporotic bone defect. These findings highlight the potential of GelHFS hydrogel as an effective therapeutic strategy for addressing challenging bone healing such as osteoporotic bone regeneration.

1. Introduction

Osteoporosis is a systemic skeletal disease characterized by progressive bone loss and the deterioration of bone tissue microarchitecture, which results in compromised bone regeneration [1–3]. Studies on bone regeneration in osteoporotic conditions has shown compromised outcomes, including diminished mechanical properties of the callus, such as reduced strength, peak failure load, and bending stiffness. Additionally, the architecture of trabecular bone is often disrupted, exhibiting reduced connectivity [4]. Basically, the compromised bone repair in osteoporosis attributed to the disease microenvironment on local MSCs and osteoprogenitors [5]. Systemic injections of MSCs

have shown promise in enhancing fracture healing, but low cell retention and the local diseased environment limit their efficacy [6]. Moreover, MSCs for tissue regeneration face challenges like changes in therapeutic behavior during *in vitro* culture [7–10]. Recent studies suggest that the benefits of MSCs are more related to their secreted factors than engraftment and differentiation [11–15]. The concept of the secretome, which encompasses all biological factors secreted by cells into the extracellular space, has emerged as a promising area in regenerative medicine. Our prior research demonstrated that the human fetal MSCs secretome (HFS) not only promotes wound healing and mitigates MSC senescence but also enhances bone consolidation [16–18]. These findings suggest significant potential for the application of MSC secretome in bone regeneration, offering a new avenue for therapeutic strategies in osteoporotic conditions.

Local delivery of bioactive factors via implanted biomaterials can significantly enhance outcomes at injury sites [19]. Hydrogels are appealing as delivery vehicles due to their tunable physical properties, biological compatibility, and potential for minimally invasive delivery [20]. A recent innovation in this field is a gelatin-based dynamic hydrogel known as GelCD, developed through host-guest complexation between gelatin and β-cyclodextrin (β-CD) [21,22]. The GelCD hydrogels exhibit excellent mechanical properties and self-healing ability. They can also retain and release both hydrophobic drugs and hydrophilic proteins, enabling sustained drug delivery [19,21]. Moreover, the dynamic crosslinks enable cell infiltration and migration, potentially favoring bone regeneration [21]. However, further improvements in the osteoinductive capacity of this GelCD hydrogels are still needed [21]. Incorporating the secretome from human fetal MSCs (HFS) into the GelCD hydrogels could potentially boost their therapeutic effectiveness, making them more suitable for applications in bone regeneration.

In the present study, we aimed to incorporate HFS into a dynamic GelCD hydrogel network to develop an optimized GelHFS hydrogel. We hypothesized that the acellular GelHFS hydrogel would create a rejuvenating environment in osteoporotic bone and subsequently enhance osteogenesis and bone regeneration through effects on endogenous MSCs behavior.

2. Materials and methods

2.1. GelCD and GelHFS hydrogels fabrication

To prepare the acrylated cyclodextrins (Ac-β-CDs), 10 g of β-CDs were dissolved in a reaction mixture of 150 mL DMF with 7 mL TEA. The mixture was stirred and cooled to 0 °C before adding 5 mL of Acryloyl chloride. After 12 h of stirring, the mixture was filtered to remove trimethylamine hydrochloride, and the remaining solution was evaporated using vacuum rotary evaporation to obtain a clear solution. The resulting modified β-CDs precipitate was dissolved in 600 mL of acetone, rinsed with acetone several times, and vacuum dried for three days. The degree of substitution (DS) was determined to be one acrylate per β-CD by ^{1}H NMR (Bruker Advance 400 MHz spectrometer) using DMSOd$_6$ with DMMA as the internal reference at 37 °C.

To create the hydrogel matrix, Ac-β-CDs were physically coupled to gelatin via host-guest interaction between the Ac-β-CDs and the aromatic residues of gelatin. Specifically, a mixture of gelatin and Ac-β-CDs was dissolved in PBS at a fixed concentration of 8 % (v/v) gelatin and 10 % (v/v) Ac-β-CDs. The initiator I2959 was added at 0.05 % (w/v), and the mixture was then pipetted into PVC molds at 37 °C and cooled to 25 °C. Finally, the mixture was exposed to 365 nm ultraviolet light (10 mW/cm^2, 10 min) at 25 °C. PVC molds of adaptable size were used for different tests [19,21,23].

To create the GelHFS hydrogel, HFS was mixed with the gel precursor and then photocrosslinked using initiator I2959. To optimize the concentration of HFS in the hydrogel, three concentration groups were established: GelHFS-L (25 µg/ml), GelHFS-M (100 µg/ml), and GelHFS-H (400 µg/ml).

2.2. Production, characterization and quantification of HFS

Human fetal MSCs (hFMSCs) were recovered from our cryopreserved stock as previously described [24]. To ensure consistency in the study, all hFMSCs used in this study were derived from the same donor, and were exclusively used at passages 3 to 5. The preparation of the human fetal MSC secretome (HFS) was modified according to existing protocols [16]. Briefly, hFMSCs were cultured in α-MEM supplemented with 10 % FBS and 1 % Penicillin-Streptomycin-Neomycin (PSN) (All from Thermo Fisher Scientific, USA). Once the cells reached 90 % confluence in 175 cm^2 culture flasks, they were washed three times with PBS to remove any residual FBS and cell debris. The cells were then incubated in 30 ml of FBS-free α-MEM for 24 h under conditions of 5 % CO$_2$ at 37 °C. After the incubation period, the conditioned media were collected, and residual cells and debris were removed by centrifugation. The supernatants were then concentrated using an Amicon Ultra-15 Centrifugal Filter Device (Millipore, USA) by centrifuging at 5000×*g* for 30 min at 4 °C. The resulting concentrated supernatant was referred to as the human fetal MSC secretome (HFS).

To determine the total protein concentration of the HFS, the Pierce™ BCA Protein Assay Kit (Thermo Fisher Scientific, USA) was used according to the manufacturer's instructions, and the protein concentration was measured by absorbance at 562 nm. The size distribution of the HFS was analyzed using dynamic light scattering (DLS) on a DelsaMax PRO Light Scattering Analyzer (Beckman Coulter, USA), which is a commonly used technique for measuring particle size in solution.

2.3. Determination of HFS released from hydrogel in vitro

GelHFS hydrogels (100 µg HFS per 1 ml GelCD precursor) were photocrosslinked in 6-mm diameter × 3-mm thickness PVC molds and then incubated in 350 µl of PBS. PBS solutions were collected and replenished at 1 h, 3 h, 6 h, 18 h, 1 day, 2 days, 4 days, 6 days, 7 days, and 14 days. The level of CD63, an exosome universal marker, in the HFS was measured using a commercial ELISA kit (System Biosciences, Palo Alto, CA) according to the manufacturer's instructions. The level of fibronectin in the HFS was measured using Human Fibronectin ELISA kit (BlueGene Biotech, Shanghai, China) according to the manufacturer's instructions.

2.4. Scanning electron microscopy

As mentioned above, samples were prepared and lyophilized. The samples were then gold-sputtered for imaging. The microstructure of the hydrogel was characterized using a Scanning Electron Microscope (Hitachi SU8010 Scanning Electron Microscope with iXRF) operating at 5 kV.

2.5. Mechanical characterization

To characterize the rheological properties of the hydrogel samples, a Kinexus Rheometer from Malvern was employed [25]. Prior to the experiments, the samples were formed and subjected to photopolymerization. The experiments were conducted at a temperature of 25 °C, and frequency sweeps were performed at 1 % strain.

2.6. Swelling ratios of the hydrogels

To determine the swelling ratios of the different dynamic hydrogels, the hydrogels were immersed in deionized water for 48 h at room temperature. Subsequently, the samples were frozen and lyophilized for 48 h. The swelling ratio was calculated using the following formula:

Swelling ratio = (*W*wet - *W*dry) / *W*dry × 100% [23].

where *W*wet and *W*dry represent the weights of the swollen and dried

hydrogels, respectively.

2.7. Rat MSCs proliferation study

MTS assay was performed to analyze the proliferative capacity of rat MSCs. MSCs derived from Sprague Dawley female rat bone marrow were isolated as we previously described [26]. MSCs at passage 2 reached 80–90 % confluence were trypsinized with 0.25 % EDTA-trypsin and seeded on a 96- well cell culture plate (Corning, German) with a density of 1×10^4 cells/ml. Cells were treated with different concentration of HFS. In indicative timepoint, 20 μl of MTS/PMS reagent (Promega, USA) was added to each well and incubated at 37 °C incubator for 4 h. The plate was read at 490 absorbance and the results were calculated according to manufacturer's protocol.

2.8. Osteogenic differentiation of rat MSCs

Rat MSCs at passage 2–4 were used in this experiemnt. Once the cell in the flask has reached 90 % confluency, it is trypsinized and plated at 4×10^5 cell/ml in a 12-well plate with basal medium. When cell monolayer reached 80 % confluency, plate was replenished with osteogenic induction medium (OIM), which is αMEM containing 10 % FBS and 1 % PSN, 10 nM dexamethasone, 50 μM ascorbic acid, and 10 mM β-glycerophosphate (all from Sigma-Aldrich, USA) and cultured at 37 °C, 5 % CO_2.

At the designated time point of osteogenic differentiation, the cell layer was washed twice with PBS and fixed with 70 % ethanol, for 5 min for ALP staining and 10 min for ARS staining. Following fixation, for ALP staining, cells were equilibrated twice with ALP buffer (0.1 M NaCl, 0.1 M Tris–HCl, and 50 mM $MgCl_2.6H_2O$, pH 9.5) for 5 min each, then incubated with a substrate solution containing 1 ml ALP buffer, 5 μl BCIP, and 10 μl NBT (Promega, USA) at 37 °C in the dark for 60 min. The ALP reaction was stopped by washing with distilled water. For ARS staining, after fixation, cells underwent three washes with ddH_2O, were stained with 0.5 % Alizarin red (pH 4.1, Sigma-Aldrich, USA) for 5 min, followed by three additional ddH_2O washes, and then allowed to air dry. Both stained plates were then scanned using an HP Scanjet G3110 Photo Scanner to visualize the results.

2.9. In vitro culture of rat MSCs-laden hydrogels

Sprague Dawley rat MSCs were expanded using complete medium consisting of α-MEM, 10 % FBS, and 1 % PSN. Cells were mixed into the hydrogel mixture at a density of 1×10^7/ml before photoencapsulation. The resulting three-dimensional (3D) culture system measured 6 mm in diameter and 3 mm in thickness, and was placed into a 12-well plate. The culture system was replenished with fresh medium every two days [25].

2.10. Live/dead cell staining

Rat MSCs were encapsulated into GelCD and GelHFS hydrogels, respectively. At indicated timepoints, the viability of the 3D cell culture samples was assessed by calcein AM (green, live cells) and ethidium bromide (red, dead cells) according to the manufacturer's protocol (Invitrogen, USA). The quantification of live cell in acquired images was analyzed by ImageJ (NIH, USA).

2.11. Cell spreading

After encapsulating rat MSCs in the hydrogel, the GelCD and GelHFS hydrogel constructs were incubated at 37 °C for 2 days. The constructs were then fixed with 4 % paraformaldehyde and stained for Vimentin, integrin β1, and counterstained with DAPI. Confocal microscopy (Nikon C2, Japan) was used to visualize the spreading of rat MSCs within the hydrogels. To quantify rat MSC spreading, Cellpose (https://www.cell

pose.org/) was utilized to segment confocal images of rat MSCs in the hydrogels. The resulting masks were analyzed using the MorphoLibJ plugin in ImageJ (NIH, USA).

2.12. Cell migration assay

The migration test was conducted using a Falcon® Permeable Support for 24-well Plate (Corning, US). GelCD and GelHFS hydrogels, each with a volume of 50 μl, were formed on the surface of the transwell membrane. The transwell inserts were then placed in a 24-well plate. Subsequently, 100 μl of media containing rat MSCs at a concentration of 2×10^6/ml were added to the top of the hydrogels, and 700 μl of growth media were added to the 24-well plates. After 24 h of incubation at 37 °C, the hydrogels were fixed with 4 % paraformaldehyde and stained with DAPI [21]. Confocal microscopy (Nikon C2, Japan) was employed to visualize the distribution of cells within the hydrogels. Quantitative analysis was performed on the obtained confocal images using ImageJ (NIH, USA). The positive intensity area of rat MSCs infiltrating the hydrogels was calculated.

2.13. Subcutaneous implantation of hydrogel in nude mice

Prior to subcutaneous implantation, two groups of rat MSC-laden hydrogels (GelCD and GelHFS, n = 3 per group) were cultured *in vitro* for 7 days in OIM as previously desbribed.

The hydrogel constructs were implanted into subcutaneous pockets of 10-week-old female nude mice obtained from the Laboratory Animal Research Center of the Chinese University of Hong Kong. All animal procedures were approved by the Animal Research Ethics Committee of CUHK (AEEC No. 19-156-TBR) and adhered to authentic vivarium conditions (25–26 °C, 70 % humidity) with free access to food and water. For subcutanous implantation, mice under general anesthesia and sterile condition were used, and then hydrogels were implanted into the subcutaneous pockets of nude mice. After 4 weeks, the mice were euthanized by fatal pentobarbital overdose. The implanted hydrogels were harvested and fixed in 4 % paraformaldehyde for further analysis.

2.14. Immunofluorescence staining

The harvested hydrogel samples from nude mice were fixed, embedded in paraffin, and sectioned at 5 μm thickness using a rotary microtome (RM2255, Leica, Germany). After deparaffinization, the sections were incubated overnight at 4 °C with primary antibodies for detecting osteocalcin (OCN, Santa Cruz, USA) and collagen I (Col I, Abcam, UK). The sections were then washed, incubated with fluorescence-conjugated secondary antibodies for 1 h at room temperature, and mounted with ProLong Gold Antifade Reagent with DAPI (Thermo Fisher Scientific, USA). Immunofluorescence imaging was performed using a Leica DM5500 fluorescent microscope (Leica, Germany). ImageJ (NIH, USA) was utilized to analyze and quantify the fluorescent signals.

2.15. Bioinformatic analysis

The proteomic dataset was obtained from our previous publication [18]. Isobaric tags for relative and absolute quantitation (iTRAQ) labeling were utilized to identify proteins in the HFS. The proteomic results were analyzed by GO database (http://geneontology.org/) to show their functional annotation. The FASTA protein sequences of HFS proteins were blasted against the online Kyoto Encyclopedia of Genes and Genomes (KEGG, https://www.genome.jp/kegg/) database to retrieve KOs, which were subsequently mapped into pathways in KEGG [27].

2.16. RNA extraction and quantitative PCR (qPCR)

Cellular samples were subjected to RNA extraction and followed by

qPCR. Total cellular RNA was extracted with RNAiso Plus reagent and reversely transcribed into cDNA by using PrimeScript RT Master Mix following the manufacturer's protocol (all from TaKaRa, Japan). The qPCR was performed by using Power SYBR Green PCR Master Mix (Applied Biosystem, USA) with QuantStudio™ 7 Flex Real-Time PCR System (Thermo Fisher Scientific, USA). Cycling condition was as follows: denaturation at 95 °C for 10 min, 40 cycles at 95 °C for 20 s, at an optimal annealing temperature for 30 s, 72 °C for 30 s, and finally at 60–95 °C with a heating rate of 0.1 °C/s. The relative fold changes of candidate genes were analyzed by using the $2^{-\Delta\Delta CT}$ method normalized to the gene expression of GAPDH. Primer sequences were shown in Table S1 [26].

2.17. Western blot

Total protein was extracted from sample using radio-immunoprecipitation assay buffer (RIPA, 25 mM Tris-Cl, pH 8.0, 150 mM NaCl, 0.1 % SDS, 0.5 % sodium deoxycholate, 1 % NP-40) supplemented with protease inhibitor and phosphatase inhibitor cocktails (Solarbio® Life Sciences, China). The lysates were centrifuged at 14,000 rpm for 10 min at 4 °C to isolate soluble protein. The soluble protein fractions were mixed with 5× sample loading buffer (Roche, USA) and boiled for 5 min. Proteins were separated by SDS-PAGE at 100 V for 2 h, then electroblotted onto polyvinylidene fluoride (PVDF) membranes at 100 V for 1 h at 4 °C. Membranes were blocked with 5 % bovine serum albumin (BSA) and probed with antibodies against TSG101, histone H3, phospho-FAK, FAK, phospho-Erk1/2, Erk1/2, β-catenin, and GAPDH. Bands were visualized using the GeneGnome XRQ system (Synoptics Group, UK) and quantitated by measuring integrated gray values using ImageJ (NIH, USA).

2.18. Animal groups and establishment of osteoporotic bone defect model

16-week-old female Sprague Dawley rats (average weight 250 g) were obtained from the Laboratory Animal Research Center of the Chinese University of Hong Kong. All animal procedures were approved by the CUHK Animal Research Ethics Committee (AEEC no. 20-136-MIS) and followed ethical regulations. For surgery, rats under general anesthesia and sterile condition were used. Bilateral ovariectomies were performed through a dorsal approach as previously described [26]. Twelve weeks after ovariectomy, cylindrical defects were created in the metaphyseal region of the distal femurs. The defects were 2.5 mm in diameter and penetrated through both sides of cortical bone. The bone defected rats were divided into 3 groups in detail below. CON: rats without implantation; GelCD: rats implanted with GelCD hydrogels; GElHFS: rats implated with GelHFS hydrogels. Rats were euthanized by fatal pentobarbital overdose at 2 and 8 weeks post-implantation (n ≥ 6 rats per group per timepoint). Femurs were harvested for analysis.

2.19. Micro-computed tomography (micro-CT) scanning

The microstructure of the distal femur was analyzed by micro-CT (vivaCT 40, Scanco Medical, Switzerland) as previously described [28]. Image acquisition was performed at 70 kV and 118 μA with a voxel resolution of 17.5 μm. Segmentation parameters were set at Gaussian sigma = 0.8, Gaussian support = 2, and threshold = 158–1000 and 211–1000 to distinguish bone from background. In addition, 75–157 Threshold was used for implanted hydrogel distinguishment.

For distal femur reconstruction, the volume of interest (VOI) contained 530 slices from the distal femur end. For the 3D reconstruction of the defect tunnel, a consistent 2 mm diameter cylindrical region of interest (ROI) with 160 slices VOI was identified. Bone volume (BV) and bone mineral density (BMD) were calculated using the manufacturer's software (Image Processing Language v4.29 d, Scanco Medical, Switzerland).

2.20. Decalcified sample analysis

Femurs were fixed in 4 % PFA at 4 °C for 48 h, followed by decalcification in 10 % ethylenediaminetetraacetic acid (EDTA) solution for 4 weeks. The decalcified samples were embedded in paraffin and sectioned at 5 μm thickness using a rotary microtome (RM2255, Leica, Germany).

For bone morphology evaluation, Goldner's trichrome staining was performed as previously described [28]. Briefly, sections were sequentially stained with Weigert's hematoxylin, Ponceau de Xylidine/acid fuchsin/azophloxin, phosphomolybdic acid/Orange G, and Light Green solutions (All from Sigma-Aldrich, USA). This differential stain contrasts mineralized bone (green), osteoid (red), calcified cartilage (light green) and nuclei (black).

For immunohistochemistry, sections were incubated with primary antibodies for integrin β1, Col I, MMP2, MMP13 (all from Abcam, UK) and OCN (SantaCruz, USA), followed by detection with a horseradish peroxidase-streptavidin system (Thermo Fisher, USA) and hematoxylin counterstaining. Brightfield microscopy images were acquired using a Leica DM5500 microscope (Leica, Germany). ImageJ (NIH, USA) was utilized to analyze and quantify positive immunostaining.

For tartrate-resistant acid phosphatase (TRAcP) staining, sections were stained by Acid Phosphatase kit (Sigma-Aldrich, USA) in accordance with the manufacturer's protocol, and then counterstained with Fast Green and Hematoxylin solutions. TRAcP-positive osteoclasts were stained in dark red and further identified as having three or more nuclei. For the analysis of TRAcP-positive osteoclasts, five fields of view at the defect site were randomly selected for each section. The N. Oc/B.Pm was analyzed using an OsteoMeasure Image Analysis System (Osteometrics, Decatur, GA, USA).

2.21. Dynamic histomorphometry

Ovariectomized rats with distal femoral defects were subcutaneously injected with fluorochromes at 10 days (calcein, 10 mg/kg, Sigma Aldrich, USA) and 4 days (xylenol orange, 90 mg/kg, Sigma Aldrich, USA) prior to sacrifice to label mineralization. At 2 weeks post defect surgery, rats were euthanized, and femurs collected. Bones were embedded without decalcification in methyl methacrylate (MMA) according to established protocols [29]. Sections of 10 μm thickness were obtained from MMA blocks using an rotary microtome (RM2255, Leica, Germany). Fluorescence microscopy images were acquired using a a Leica DM5500 microscope (Leica, Germany) and analyzed using ImageJ (NIH, USA) to quantify new bone formation.

For Von kossa staining, the sections were incubated in 1 % AgNO_3 solution under UV light for 1 h to detect calcium deposits. The sections were then washed in distilled water, treated with 5 % Na_2S_2O_3 for 5 min to remove unreacted silver, and rinsed again in distilled water. Counterstaining was performed with nuclear fast red. Brightfield microscopy images were acquired using a Leica DM5500 microscope (Leica, Germany). ImageJ software (NIH, USA) was utilized to analyze and quantify the area of silver deposit.

2.22. Biomechanical test

The biomechanical properties of femurs implanted with hydrogel constructs were evaluated at 8 weeks post-implantation. Following established protocols [30], the proximal end of each femur was embedded in a polymer resin (Ureol 2020, Ciba Specialty Chemicals, Hong Kong) and mounted on a material testing machine (H25KS, Hounsfield Test Equipment Ltd., UK) oriented at 25° above the horizontal plane. A compressive force was applied to the femoral metaphysis directly above the defect site at a constant velocity of 25 mm/min using a metal blade until failure occurred. Load-displacement curves were generated from which the ultimate load (N) and stiffness (N/mm) were determined. Data acquisition and analysis were performed using the
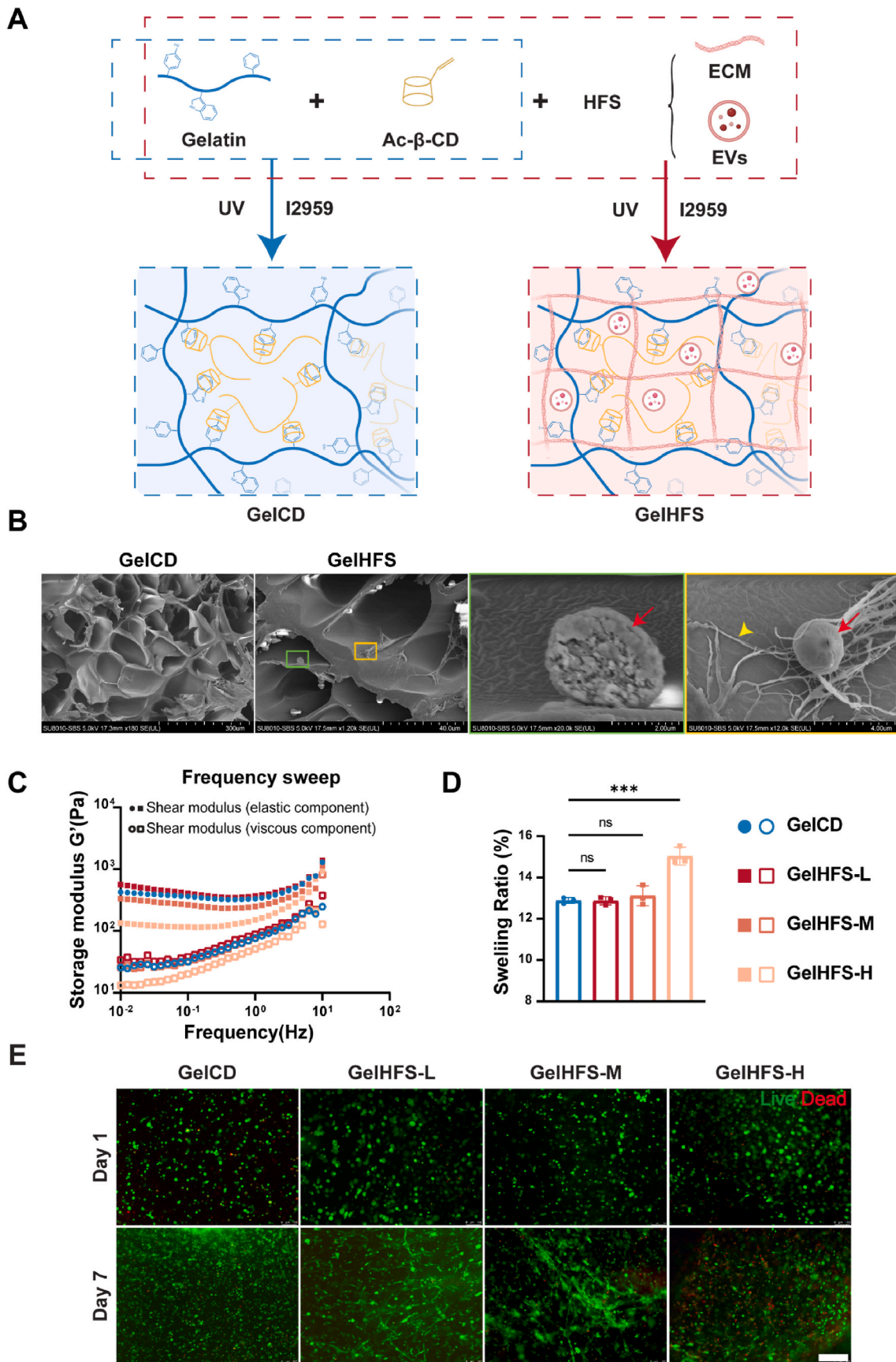
(caption on next page)

Fig. 1. Formation and properties of GelCD and GelHFS hydrogels. (A) Schematic illustration of the formation of GelCD and GelHFS hydrogels. Left panel (blue dashed line) shows GelCD hydrogel formation involving gelatin and Ac-β-CD under UV light with I2959 initiator, resulting in a network through reversible host-guest complexation. Right panel (red dashed line) depicts GelHFS hydrogel formation, which includes GelCD and HFS (consists of ECM and EVs), followed by photo-crosslinking under UV light with I2959, leading to a more complex hydrogel network. **(B)** SEM images demonstrate the microstructure of GelCD and GelHFS hydrogels. The green and yellow rectangles in the GelHFS image correspond to the magnified images. Red arrows indicate aggregated EVs while yellow arrowhead indicates ECM. The scale bars in the images are 300 μm, 40 μm, 2 μm, and 4 μm from left to right, respectively. **(C)** Represent frequency sweep curve of GelCD and GelHFS with various HFS concentrations. **(D)** The swelling ratio of GelCD and GelHFS with various HFS concentrations. Data are presented as mean values ± SD, n = 3 independent hydrogels per group, ***$P < 0.001$, ns indicates no statistical difference (one-way ANOVA with Tukey's HSD). **(E)** Representative live/dead staining images of rat MSCs encapsulated within hydrogels after 1 and 7 days of culture. Scale bar = 100 μm. GelHFS-L: GelCD hydrogel with a low concentration of HFS incorporated, GelHFS-M: GelCD hydrogel with a medium concentration of HFS incorporated, GelHFS-H: GelCD hydrogel with a high concentration of HFS incorporated.

built-in software (QMAT Professional Material Testing Software, Hounsfield Test Equipment, UK).

2.23. In vitro and in vivo degradation of hydrogel

For *in vitro* degradation, GelCD and GelHFS hydrogels were formed and incubated in PBS at 37 °C for 1, 3, 5, 7, and 14 days. At each timepoint, hydrogels were harvested, frozen, lyophilized, and weighed. The dry mass was measured following lyophilization to quantify degradation.

For *in vivo* degradation, fluorescent GelCD and GelHFS hydrogels were implanted subcutaneously in nude mice. Fluorescein isothiocyanate (FITC)-conjugated gelatin was synthesized as previously described [31] and used to prepare fluorescent hydrogel constructs. *In vivo* fluorescence imaging was performed at 1, 2, 3, 7, 9, 10, 11, 12, and 13 days post-implantation using an IVIS imaging system (IVIS 200, Caliper Life Sciences, USA). Fluorescence intensity was quantified to assess degradation of implanted hydrogels over time.

2.24. Statistical analysis

All the cellular experiments were repeated at least 3 times with 3 biological replicates. A priori power analysis (G*Power, Universität Düsseldorf) based on the previous studies using a similar rat bone defect model in evaluating a bone graft performance determined that a sample size of 6 was needed to obtain 90 % statistic power at the significance value of 0.05 when comparing quantitative μCT analyses outcome. All results were shown as mean ± standard deviation (SD). Statistical analysis was performed by GraphPad Prism (GraphPad Software, USA). Pair-wise comparisons passing normality test were analyzed with Student's t-test. Multiple comparisons passing normality test were analyzed with ANOVA and post hoc Tukey's multiple comparisons test.

3. Results

3.1. Dynamic hydrogel with human fetal MSCs secretome (GelHFS) exhibits favourable mechanical properties and biocompatibilities

The fabrication of GelCD and GelHFS hydrogels was shown in Fig. 1A. First, acryloyl β-cyclodextrin (ac-β-CD) was synthesized and the degree of substitution of β-CD was 1.0 (Supplementary Fig. 1). And then ac-β-CD was used as the host monomer to form reversible host-guest complexes with aromatic residues in gelatin via a photo-polymerization process (Fig. 1A), yielding the host-guest hydrogels, referred to as GelCD hydrogels. We also produced GelHFS hydrogels by incorporating HFS into the GelCD precursor (Fig. 1A). Notably, the quality of HFS was controlled from batch to batch (Supplementary Fig. 2). SEM images of both GelCD and GelHFS hydrogels are presented in Fig. 1B, demonstrating that both hydrogel types exhibit a porous structure with macropores approximately 100 μm in diameter. Moreover, we observed the presence of HFS components including proteins and extracellular vehicles (EVs), homogeneously distributed within the hydrogel while maintaining their nanosphere morphology.

We evaluated the release kinetics of CD63 and fibronectin from the

hydrogel to quantify the release profiles of different components from HFS since it is a heterogenous population. CD63 is a protein enriched in EVs while fibronectin is a representative extracellular matrix (ECM) protein. As demonstrated in Supplementary Fig. 3, the GelHFS hydrogel facilitated a consistent release of HFS over a period of 14 days *in vitro*. The maximum release rates for CD63 and fibronectin were 62.26 % ± 5.13 and 34.38 % ± 0.66, respectively.

We then optimized the concentration of HFS for the incorporation of GelCD hydrogel. Biomechanical properties were assessed, and we found that GelHFS-L (25 μg/ml) and GelHFS-M (100 μg/ml) did not affect the storage modulus and swelling ratio of the hydrogels (Fig. 1C and D). However, high concentrations of HFS (GelHFS-H (400 μg/ml)) resulted in a reduction in the storage modulus of GelHFS-H hydrogels and an increase in its swelling ratio. After 7 days of culture, the GelHFS-L hydrogel demonstrated a high viability rate for the encapsulated rat MSCs, with the majority (93.67 % ± 1.38) of cells remaining viable (Fig. 1E & Supplementary Fig. 4). Furthermore, HFS at concentrations ranging from 25 to 100 μg/ml showed to enhance osteogenesis in rat MSCs without impairing their proliferation, as demonstrated in Supplementary Fig. 5. Based on these findings, the low concentration of HFS was selected as the optimized concentration for incorporating GelCD hydrogels. This concentration provided an adequate balance between the potential benefits of HFS incorporation and the effects on hydrogel properties.

3.2. GelHFS hydrogel promotes spreading, migration and osteogenic differentiation of MSCs

We investigated the behaviors of rat MSCs encapsulated in GelCD and GelHFS hydrogels. Confocal microscopy imaging was used to reconstruct the 3D structure of encapsulated cells, which showed that rat MSCs in GelHFS hydrogels had more substantial spreading and cytoskeletal intermediate filament (vimentin) compared to those in GelCD hydrogels (Fig. 2A). AS showed in Fig. 2B, cells in GelHFS group demonstrated spindle MSCs-like shape (0.52 ± 0.15) while cells in GelCD group exhibited spherical morphologies (0.98 ± 0.016). Additionally, the area per cell in GelHFS groups was significantly larger than that in GelCD groups (Fig. 2C).

To investigate the ability of GelHFS hydrogels to promote cell migration, we seeded rat MSCs onto the surface of hydrogels. After 24 h of culture, we observed that nearly all MSCs infiltrated and migrated into the GelHFS hydrogels. In contrast, most MSCs remained on top of the GelCD hydrogels (Fig. 2D and E).

We then evaluated the osteogenic differentiation of rat MSCs in the GelCD and GelHFS hydrogels *in vivo* by implanting the rat MSCs laden hydrogels into subcutaneous pockets in nude mice for 4 weeks (Fig. 2F& Supplementary Fig. 6). Results revealed mor positive signals for OCN and Col I immunostaining in the GelHFS group, compared with those in the GelCD group (Fig. 2G–I). These findings collectively suggest that the GelHFS hydrogels provide a favourable microenvironment for efficient cell spreading and infiltration *in vitro*. Furthermore, *in vivo* experiments demonstrate that GelHFS hydrogels promote osteogenic differentiation of encapsulated rat MSCs, indicating their potential for use in bone tissue engineering applications.
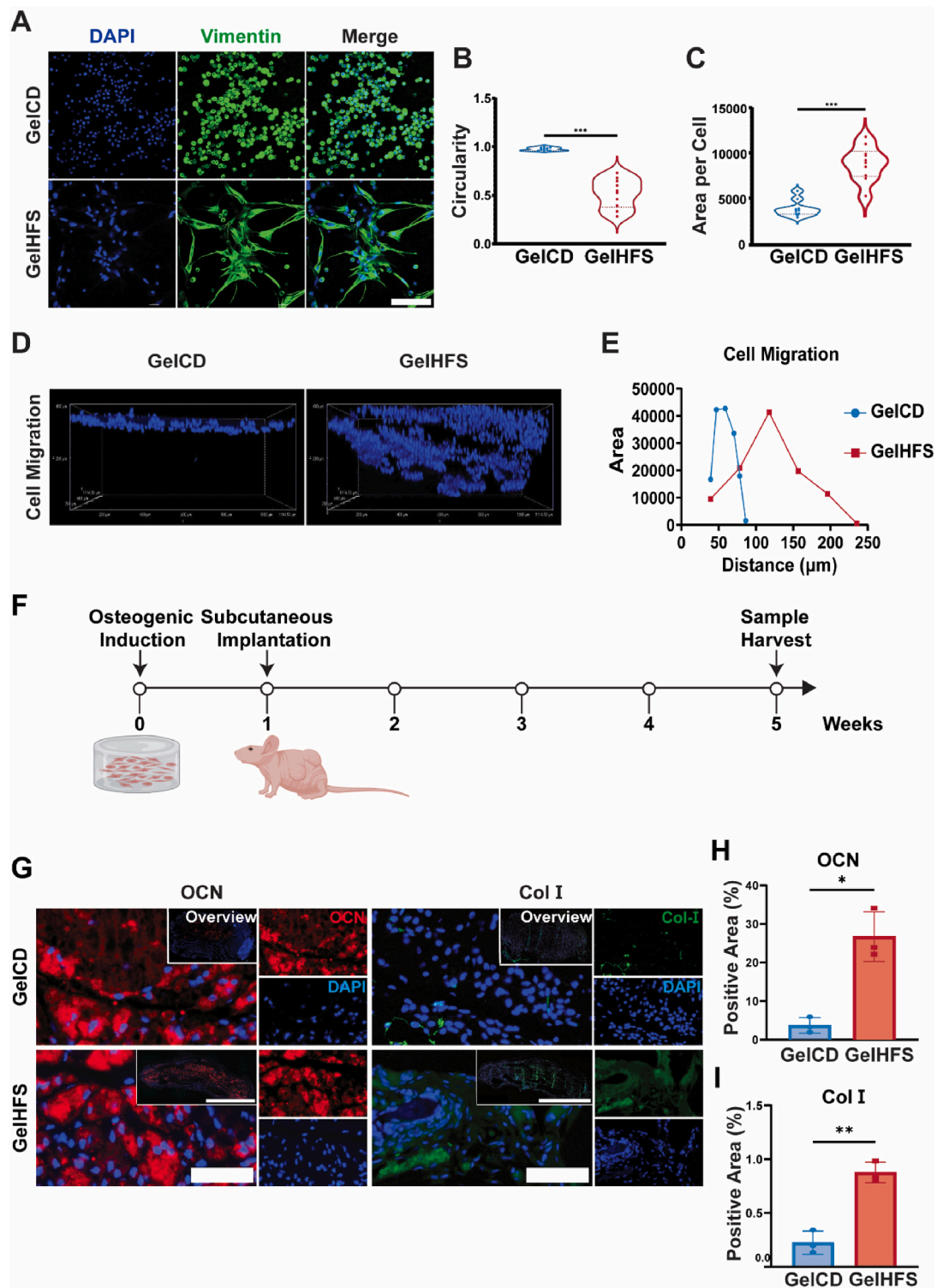
Fig. 2. GelHFS hydrogel presents conducive biological properties. (A) Representative images show rat MSCs encapsulated in GelCD and GelHFS hydrogels on culture day 2, stained for vimentin (green) and nuclei (blue). The scale bar is 100 μm. **(B&C)** The circularity and area of the rat MSCs encapsulated within the GelCD and GelHFS hydrogels, respectively. Circularity values range from 0 (highly elongated) to 1 (perfectly circular). Data are presented as mean values $\pm$ SD, n = 10 cells per group, ***$P < 0.001$ (two-tailed Student's t-test). **(D)** Confocal images demonstrate the 3D distribution of DAPI-stained rat MSC nuclei within GelCD and GelHFS hydrogels after 24 h of *in vitro* culture. **(E)** Invasion distance of DAPI-stained rat MSCs nuclei clusters within the GelCD and GelHFS hydrogels. The scanning depth for (D) was 400 μm. **(F)** Timeline of ectopic bone formation assay. Rat MSCs encapsulated in GelCD and GelHFS were cultured in osteogenic induction medium for 7 days before subcutaneous implantation in nude mice. After 4 weeks post-implantation, samples were harvested for analysis. **(G)** Immunofluorescence staining against OCN (red) and Col I (green) of rat MSCs-laden GelCD and GelHFS after 4 weeks of subcutaneous implantation in nude mice. Nuclei were stained with DAPI. Scale bar = 100 μm. Overview: the morphology of rat MSCs encapsulated hydrogels after 4 weeks of implantation in nude mice. Scale bar = 1 mm. **(H&I)** Quantification of integrin β1 and Col I intensity in (G). Analysis was performed using ImageJ software. Data are presented as mean values $\pm$ SD, with n = 3 independent hydrogels per group. *$P < 0.05$, **$P < 0.01$ (two-tailed Student's t-test).
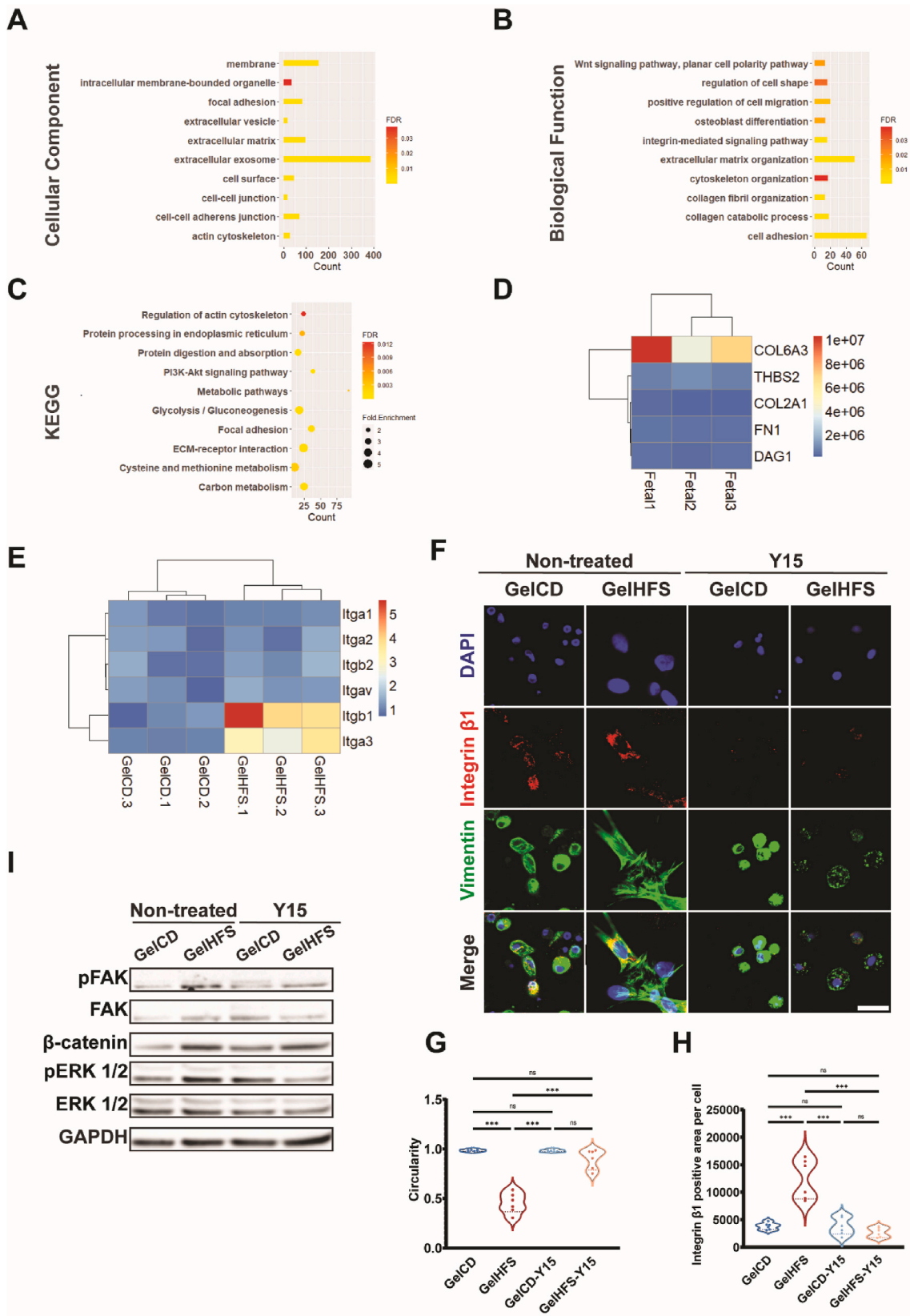
(caption on next page)

Fig. 3. GelHFS hydrogel potentially activated integrin β1 induced focal adhesion pathway. (A) GO annotation (cellular component) of HFS proteins. **(B)** GO annotation (biological function) of HFS proteins. **(C)** KEGG enrichment of HFS proteins. **(D)** Heatmap of Top 5 HFS proteins which annotated into extracellular matrix GO term in (A). **(E)** The gene expression levels of integrin subunits *Itga1*, *Itga2*, *Itga3*, *Itgav*, *Itgb1*, and *Itgb2* were measured by qPCR in rat MSCs-laden GelCD and GelHFS after 2 days of culture. The data represents the relative expression levels normalized to *GAPDH* and expressed as fold change compared to the expression levels in rat MSCs-laden GelCD. **(F)** Cell spreading in GelCD and GelHFS hydrogels after 2 days of culture with or without treatment with FAK inhibitor Y15. Representative images show integrin β1 (red), vimentin (green) and nuclei (blue) staining. Scale bar = 15 μm. **(G)** The circularity of rat MSCs in (F) was quantified using ImageJ software. Circularity values range from 0 (highly elongated) to 1 (perfectly circular). Data are presented as mean values ± SD, with n = 6 cells per group. ***$P < 0.001$, ns indicates no statistical difference (one-way ANOVA with Tukey's HSD). **(H)** Quantification of positive area of integrin β1 in (F) was performed using ImageJ software. Data are presented as mean values ± SD, with n = 6 cells per group. ***$P < 0.001$, ns indicates no statistical difference (one-way ANOVA with Tukey's HSD). **(I)** The protein expression levels of pFAK, total FAK, β-catenin, pERK1/2, ERK1/2, and GAPDH were analyzed in rat MSCs encapsulated in GelCD and GelHFS in the absence or presence of FAK inhibitor Y15. Protein expression was quantified by Western blotting.

3.3. HFS activates integrin β1 mediated focal adhesion pathway

In order to analyze the protein compositions in HFS, we conducted a proteomic analysis of HFS and found that the majority of HFS components originated from the extracellular exosome (55.6 %) and extracellular matrix (13.8 %) (Fig. 3A). Interestingly, a significant proportion of HFS proteins (13 %) was annotated for extracellular matrix organization, while 2 % of HFS was annotated for integrin-mediated signaling pathway (Fig. 3B). KEGG pathway analysis revealed that HFS was also annotated for focal adhesion pathway (5 %) and ECM-receptor interaction (3 %, Fig. 3C). Additionally, we identified significant ECM proteins in HFS (Fig. 3D). All of them can interact with integrins. Our hypothesis thus far is that the beneficial effect on MSCs behavior and osteogenesis in GelHFS hydrogels could attributed to activated focal adhesion pathway by upregulating integrins.

To determine which integrin subunit was regulated by HFS, we examined the mRNA expression of integrin subunits in rat MSCs encapsulated in GelCD and GelHFS hydrogels. Our results showed that GelHFS hydrogels upregulated the gene expression of *Itgb1* by 5-fold ($P < 0.01$) and *Itga3* expression by 4-fold ($P < 0.01$) compared to the GelCD group (Fig. 3E). The up-regulated protein expression of integrin β1 of rat MSCs in GelHFS hydrogels was further confirmed via immunofluorescent staining (Fig. 3 F–H). Noteworthy, this enhancement was abolished by Y15 which inhibits the phosphorylation of FAK. Furthermore, Western Blot results confirmed that GelHFS hydrogels increased the protein expression of β-catenin and activated FAK-ERK signaling pathway of cultured rat MSCs, while such increase was abolished by FAK inhibitor Y15 (Fig. 3I).

In summary, our findings demonstrate that the GelHFS hydrogels induce rapid cell spreading and osteogenic differentiation, and these beneficial effects could be facilitated by the interaction between integrin β1 of rat MSCs and HFS (ECM components).

3.4. GelHFS hydrogel promotes bone regeneration in an osteoporotic bone defect model

In this study, we evaluated the effectiveness of GelHFS hydrogels in facilitating bone regeneration in osteoporotic conditions induced by ovariectomy in female rats (Fig. 4A). The progression of osteoporosis was confirmed prior to hydrogel implantation (Supplementary Fig. 7). Micro-CT analysis revealed rare bony tissue in the control group at both 2- and 8-weeks post-surgery. In contrast, the GelCD group displayed new bone formation within the defect site, while the GelHFS group exhibited significantly greater bone-like tissue formation as early as two weeks, with substantial mineralization evident by eight weeks (Fig. 4B–E and Supplementary Fig. 8). Biomechanical testing showed that the GelHFS hydrogels not only supported bone healing but also improved biomechanical properties (Fig. 4F and G). The stiffness and ultimate load in the GelHFS group were significantly higher compared to those in the GelCD group, with statistical significance ($P < 0.05$ for both parameters).

Histological analysis using Goldner's trichrome staining provided insights into the tissue morphology within the defect sites at 2- and 8-weeks post-surgery (Fig. 4H). The control group showed almost no new bone formation throughout the study period. The GelCD group

demonstrated a mix of hydrogel matrix and fibrous tissue with emerging woven bone at two weeks, which remained marrow and fat tissue by 8 weeks. Remarkably, in the GelHFS group, woven bone had largely replaced the hydrogel and fibrous tissue by 2 weeks, and by 8 weeks, this had remodelled into mature lamellar bone. Furthermore, there was very little hydrogel remained at the defect site. In addition, GelHFS group did not showed superior effect on osteoclast inhibition compared to GelCD group (Supplementary Fig. 9).

These results collectively demonstrate that GelHFS hydrogels significantly enhance the regeneration of osteoporotic bone defects, including promoting new bone formation and increasing bone mechanical properties.

3.5. GelHFS hydrogel recruits integrin $\beta1^+$ endogenous cells into the defect site

To observe dynamic new bone formation, *in vivo* double labels of calcein and xylenol were measured (Fig. 5A). In details, we injected calcien and xylenol at day 4 and day 10 post-implantation and harvested samples at day 14 post-implantation. On day 10 post-surgery, there was little bony tissue formation, but a sudden increase was observed on day 14 (Fig. 5B). Furthermore, there was no statistical difference in bone formation between the GelCD and GelHFS groups on 10 days post-surgery, but a significant increase in newly formed tissue was observed in the GelHFS group compared to the GelCD group on day 14 ($P < 0.05$, Fig. 5D).

We next investigated the expression of integrin β1, OCN and Col I at the defect site using consecutive sections (Fig. 5C). According to the semiquantitative results (Fig. 5E–G), the GelHFS group exhibited significantly more intense positive staining against integrin β1, OCN and Col I at the defect site compared to the GelCD group ($P < 0.001$, $P < 0.01$ and $P < 0.05$, respectively). The results confirmed that GelHFS hydrogel recruited more integrin β1 expressing cells to the defect site, and promoting the osteogenesis of endogenous cells which leads to more bone matrix deposition.

3.6. GelHFS hydrogel exhibits faster degradation in osteoporotic bone

Given that GelHFS recruited endogenous cells to the defect site, we speculated that the recruited cells mediate faster hydrogel degradation, which further promotes cell infiltration and *in situ* bone regeneration.

In order to compare the degradation behavior of GelCD and GelHFS hydrogels, we conducted *in vitro* and *in vivo* experiments. *In vitro*, both groups showed a gradual decrease in weight over time, with no significant difference in weight loss between the GelCD and GelHFS groups (Fig. 6A). In details, 6.58 % ± 0.26 and 6.03 % ± 0.50 of the original weights in the GelCD and GelHFS groups remained in day 14, respectively. We next investigated the degradation behavior *in vivo*, we used FITC-conjugated gelatin to form GelCD and GelHFS hydrogels and subcutaneously implanted them in nude mice. We found no significant difference in degradation between GelCD and GelHFS hydrogels for 2 weeks post-implantation (Fig. 6B and C).

However, micro-CT revealed that after implanting in the distal femur, GelHFS hydrogels degraded significantly faster than GelCD at 2
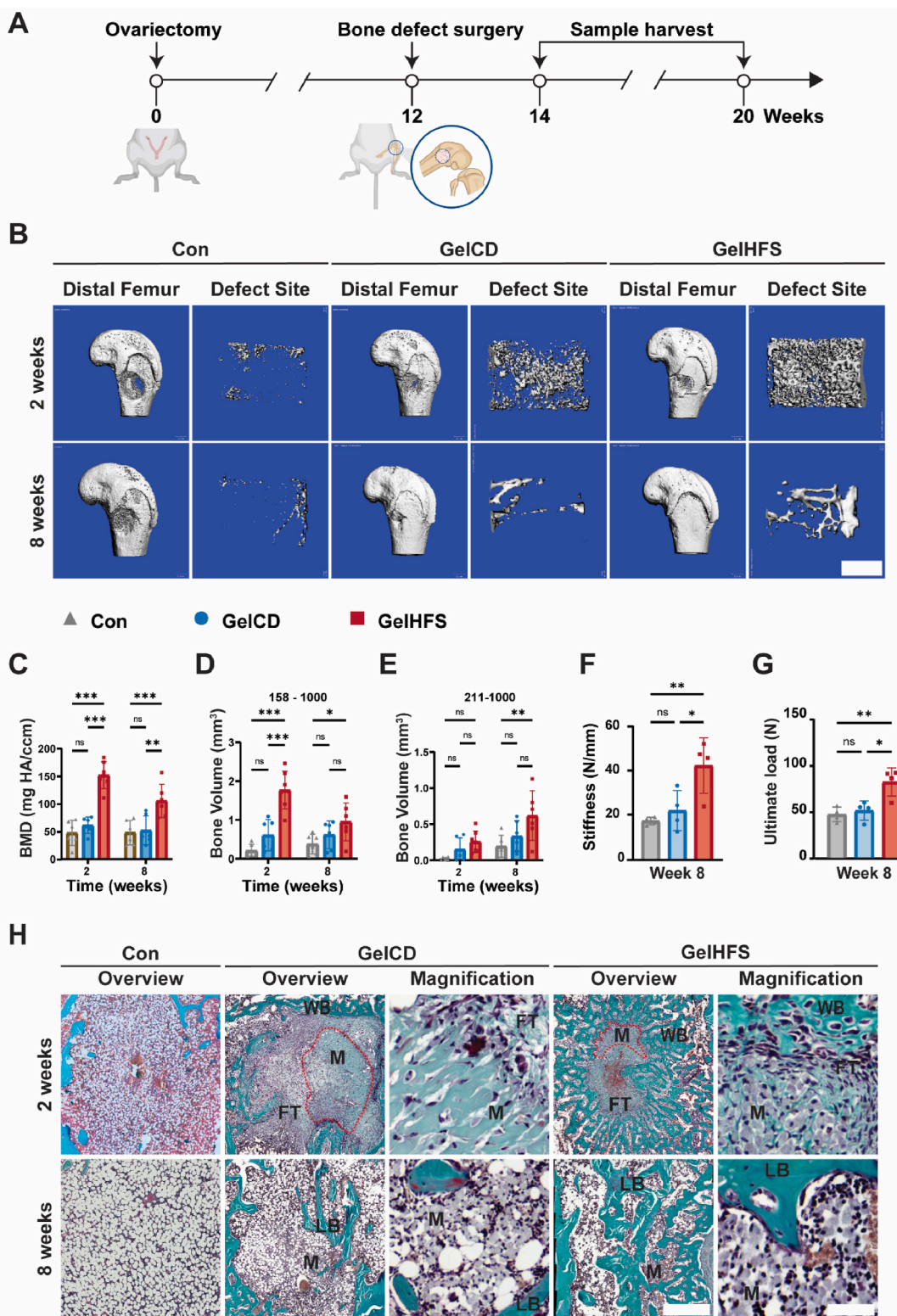
Fig. 4. GelHFS hydrogel promotes osteoporotic bone regeneration. (A) Timeline of bone defect surgery. Female rats underwent ovariectomy to induce an osteoporotic condition for 12 weeks. Afterward, they underwent defect surgery on the distal femur with or without hydrogel implantation. Samples were harvested 2- and 8-weeks post-implantation for analysis. **(B)** Three-dimensional reconstructed mineralized tissue in the defect tunnels of distal femurs at 2 and 8 weeks after implantation. The scanning resolution is 17.5 μm at 70 kV, 114 μA. Scale bar = 1 mm **(C ~ E)** Quantitative data of micro-CT analysis. Quantitative analysis of the BMD (C). Thresholds of 158–1000 were used to represent total mineralized tissue (D), and thresholds of 211–1000 were used to represent mineralized tissue undergoing remodeling process (E). Data are presented as mean values ± SD, with n ≥ 6 rats per group per timepoint. ns indicates no statistical difference, *$P < 0.05$, **$P < 0.01$, ***$P < 0.001$ (one-way ANOVA with Tukey's HSD). **(F&G)** Biomechanical properties of distal femur at 8 weeks post-implantation. The stiffness (F) and ultimate load (G) were measured using a mechanical testing machine. Data are presented as mean values ± SD, with n = 4. *$P < 0.05$ (two-tailed Student's t-test). **(H)** Goldner's trichrome staining of the defect site in the distal femur of OVX rats, n = 4 per group. The red dashed area indicates the remaining hydrogels within the defect site. M: materials. WB: woven bone. LB: lamellar bone. FT: fibrous tissue. Scale bar = 500 μm for overviewed images and 50 μm for magnified images.
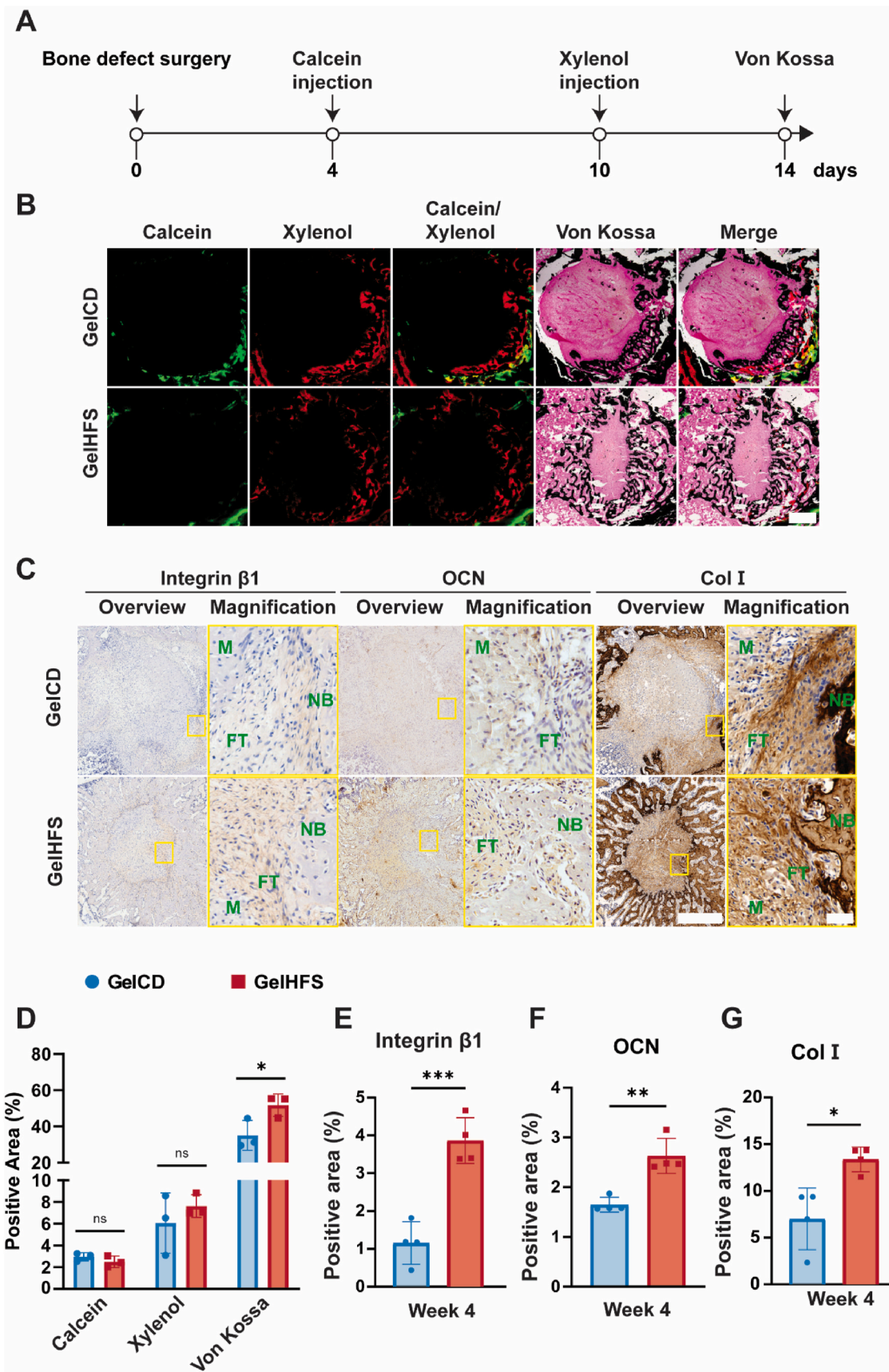
(caption on next page)

Fig. 5. GelHFS hydrogel recruits endogenous cells into the defect site to promote bone regeneration. (A) Timeline of fluorescence labeling for (B). Female rats underwent defect surgery on the distal femur and were implanted with hydrogels. Calcein and xylenol were injected at day 4 and 10 post-implantation, respectively. Samples were harvested at 2 weeks post-implantation for analysis. **(B)** Representative calcein/xylenol fluorescence microscopic images and Von Kossa staining images for assessment of bone formation at 2 weeks after hydrogel implantation. Scale bar = 200 μm. **(C)** Representative IHC images of defect site at 2 weeks post implantation. Integrin β1, OCN and Col I were stained on adjacent sections 5 μm apart. The yellow rectangles in the overview images correspond to the magnified images. NB: new bone. FT: fibrous tissue. M: materials. Scale bar = 500 μm for overview and 50 μm for magnification. **(D)** Quantification of positive area in (B) analyzed by ImageJ software. Data are presented as mean values ± SD, with n = 3. *$P < 0.05$, and ns indicating no statistical difference (two-tailed Student's t-test). **(E ~ G)** Quantification of integrin β1, OCN and Col I intensity in (C) was performed using ImageJ software. Data are presented as mean values ± SD, with n = 4. *$P < 0.05$, ***$P < 0.001$ (two-tailed Student's t-test).

weeks post-surgery ($P < 0.05$, Fig. 6D & E). Furthermore, immunohistology staining showed that there are more matrix metalloproteinases such as MMP2 and MMP13 expression in the GelHFS implantation than that in the GelCD group (Fig. 6F–H). These findings suggest that the faster degradation ability of GelHFS hydrogels attributed by endogenous cells secreted MMPs.

4. Discussion

In the present study, we introduce the development of a novel GelHFS hydrogel, in which the HFS is incorporated into the GelCD hydrogel. GelHFS hydrogel retains biomechanical properties equivalent to GelCD hydrogel while promoting cell spreading, migration, and osteogenic differentiation of encapsulated MSCs. Furthermore, the acellular GelHFS hydrogel facilitates bone regeneration in an osteoporotic bone defect model by recruiting integrin β1$^+$ endogenous cells and activating integrin β1 induced focal ashesion pathway. This supports our hypothesis that the acellular GelHFS hydrogel would create a rejuvenating environment in osteoporotic bone, thereby enhancing osteogenesis and bone regeneration via influences on endogenous cell behavior (Fig. 7).

GelCD hydrogel was developed using host-guest complexation between gelatin and β-CD. The weak host-guest crosslinking facilitates the infiltration and migration of cells into the hydrogels, and the excess β-CDs enable hydrogel-tissue adhesion and enhance the loading and sustained delivery of hydrophobic drugs [23]. Previous studies show demonstrate that GelCD hydrogel is more superior than methacrylated gelatin hydrogels (a covalently crosslinked gelatin hydrogels). For example, GelCD hydrogels could encapsulate and sustain the release of hydrophobic drugs like dexamethasone more effectively than methacrylated gelatin hydrogels [23]. Furthermore, GelCD hydrogels was reported to emulate the intrinsic structural dynamics of the ECM. Compared to methacrylated gelatin hydrogels with similar stiffness and biodegradability, GelCD hydrogels significantly promote the clonal expansion and viability of encapsulated mouse ESCs [22]. Previous findings highlight the critical role of the structural dynamics of the hydrogel matrix in supporting infiltration and migration of encapsulated cells.

Despite GelCD hydrogel's excellent biocompatibility both *in vitro* and *in vivo*, enhancements in its osteoinductive capacity are necessary. Previously, we found that GelCD hydrogels containing MSCs and icaritin effectively maintained BMD and facilitated bone regeneration in a model of steroid-associated osteonecrosis. However, this effect was absent in the groups using only GelCD or GelCD with icaritin, underscoring the significant role of encapsulated MSCs [21]. In another previous study, the incorporation of chondrogenic agents (kartogenin and TGF-β1) with stem cells into GelCD hydrogel significantly enhanced its chondroconductivity. Using a rat osteochondral defect model, this hybrid hydrogel effectively promoted the regeneration of both hyaline cartilage and subchondral bone. These findings suggest that GelCD hydrogel is a promising biomaterial for the delivery of therapeutic agents and cells, supporting its potential in advanced stem cell therapies [19]. However, given the challenges associated with MSCs treatment, including low cell retention and diminished efficacy in diseased environments [6], we are pursuing the development of an acellular hydrogel for bone regeneration.

Secretome can be defined as a set of biological factors that are secreted from cells into the extracellular space, including soluble factors (growth factors, cytokines, chemokines, and enzymes) and EVs that transport lipids, proteins, and RNA and DNA subtypes [32–34]. The EVs are heterogeneous populations of phospholipid bilayer membrane-bound vesicles that may be grouped into exosomes (30–120 nm), microvesicles (100–1000 nm), and apoptotic bodies (500–2000 nm) based on their size and cellular origin [35–37]. Research on the application of stem cell secretome in orthopaedics has grown in recent years. One study incorporated human umbilical cord-derived mesenchymal stem cell (hUCMSC) secretome into silk fibroin-based hydrogels, which were injected into the tibial bone marrow cavity of osteoporotic rats. This transplantation strategy delayed local bone loss by increasing bone mass and trabecular structure, potentially due to the anti-senescence effects of hUCMSC secretome [38]. Beside umbilicus, researchers also study secretome derive from other tissues/cells. Our previous study compared HFS and human adult MSCs secretome (HAS) in different applications and suggest that HFS has superior effects than HAS. Evidence demonstrated that compared to HAS, HFS downregulated the pro-apoptotic gene Bax as well as senescence-associated genes p53 and p16 of senescent cells [16]. Furthermore, HFS significantly enhanced wound healing by promoting vascularization and inhibiting inflammation in the streptozotocin -induced diabetic rat model in comparison of HAS [18]. We also showed osteogenic promoting effect of HFS in a distraction osteogenesis model [17]. Considering the beneficial effects of HFS, we speculated that it could facilitate osteoporotic bone regeneration.

Osteoporotic bone fracture/defect healing poses significant clinical challenges, prompting numerous studies aimed at accelerating healing period and enhancing healing outcome. One such study introduced bisphosphonate-functionalized injectable hydrogel microspheres (GelMA-BP-Mg). These microspheres utilized a metal ion ligand coordination reaction to capture magnesium ions (Mg^{2+}), facilitating the reconstruction of cancellous bone in osteoporotic defects, visible from 4 weeks post-surgery [39]. Further advancements were made in another study that developed nano-hydroxyapatite, resveratrol, and chitosan composite microspheres designed to sustain local release of resveratrol. When these microspheres were implanted into bone defects in osteoporotic rat femoral condyles, they enhanced bone regeneration, with initial signs of healing observed at six weeks post-surgery [40].

Contrasting these findings, our research with GelHFS hydrogel demonstrated more rapid osteoporotic bone healing. When applied to femoral defects in osteoporotic rats, the GelHFS hydrogel showed significant new bone formation as early as 2 weeks post-surgery. This is equal to the healing timeline in studies involving normal, non-osteoporotic rats, which also showed recovery at two weeks post-surgery [41]. This rapid effectiveness is particularly crucial for osteoporotic patients since osteoporotic fracture often demonstrated delayed healing [5].

The beneficial effects of GelHFS hydrogel in osteoporotic bone regeneration primarily stem from two mechanisms. First, GelHFS effectively recruits endogenous MSCs to the defect site, enhancing bone regeneration through engagement with the integrin β1-induced focal adhesion pathway. Second, recruited MSCs accelerate the degradation of the hydrogel, enhancing in situ bone regeneration.

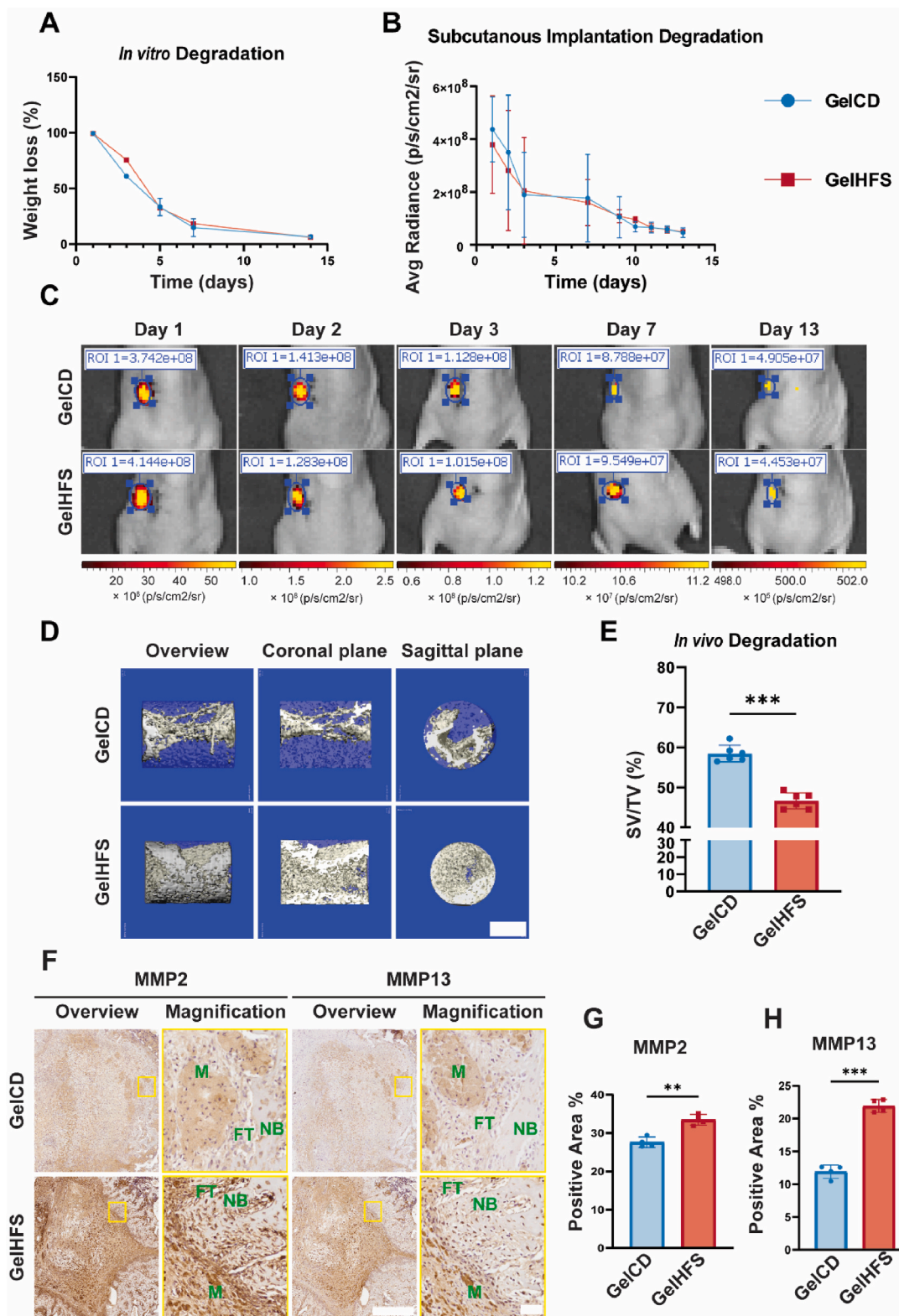Our results indicate that GelHFS hydrogel upregulates integrin β1

Fig. 6. GelHFS hydrogel exhibits faster degradation in osteoporotic bone. (A) Weight loss of GelCD and GelHFS hydrogels *in vitro* over time. Data are presented as mean values ± SD, with n = 3. $P > 0.05$ (two-tailed Student's t-test). **(B)** Changes in fluorescence of hydrogels implanted in nude mice, as measured by *in vivo* imaging system. Data are presented as mean values ± SD, with n = 3. $P > 0.05$ (two-tailed Student's t-test). **(C)** Representative *in vivo* fluorescence intensity images of hydrogels. **(D)** Residual hydrogels at the defect site of rats at 2 weeks post hydrogel implantation, as visualized by blue color. White color indicates mineralized tissue. Scale bar = 1 mm. **(E)** Percentage of scaffold volume (SV) to total volume (TV) in (D), quantified by micro-CT analysis. Data are presented as mean values ± SD, with n = 6. ***$P < 0.001$ (two-tailed Student's t-test). **(F)** Representative IHC images of defect site at 2 weeks post implantation. MMP2 and MMP13 were stained on adjacent sections 5 μm apart. The yellow rectangles in the overview images correspond to the magnified images. NB: new bone. FT: fibrous tissue. M: materials. Scale bar = 500 μm for overview and 50 μm for magnification. **(G&H)** Quantification of MMP2 and MMP13 intensity in (F) was performed using ImageJ software. Data are presented as mean values ± SD, with n = 4. **$P < 0.01$, ***$P < 0.001$ (two-tailed Student's t-test).
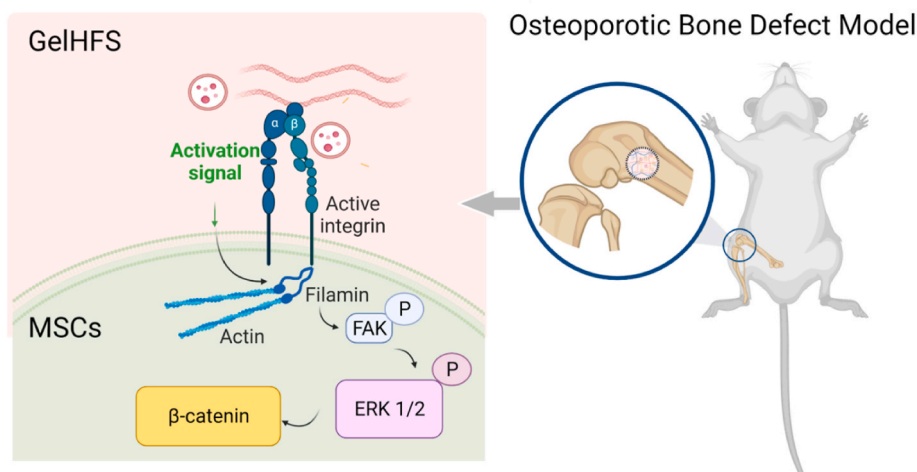
Fig. 7. GelHFS hydrogel creates a rejuvenating stem cell niche and enhances osteoporotic bone regeneration via activating integrin mediated focal adhesion pathway.

and β-catenin protein expression and activates the focal adhesion pathway, involving FAK and ERK1/2. This evidence supports the hypothesis that GelHFS hydrogel attracts endogenous MSCs and promotes their osteogenesis through the integrin β1 pathway. The ECM components of HFS, including collagens, thrombospondins, and fibronectin, likely adhere these endogenous cells due to their known interactions with integrins [42]. Binding of ECM components to integrins triggers FAK and ERK1/2 phosphorylation on MSCs, which is vital for osteogenic differentiation [43–45].

Our research provides robust evidence to support the second mechanism. Firstly, GelHFS hydrogel facilitates the spreading and migration of MSCs, as demonstrated *in vitro*. Histological analysis further confirms this, showing large amount of bone matrix but a very small amount of residual hydrogel material at the defect sites. Additionally, IHC staining reveal higher levels of integrin β1, osteocalcin, collagen I, MMP2, and MMP13 in the GelHFS group. These proteins are secreted by MSCs and osteoblasts, playing a crucial role in bone formation [46]. Notably, MMP2, which are matrix metalloproteinases, specifically degrade gelatin, a component of GelHFS hydrogel [47]. MMP2 and MMP13 lead to a faster degradation rate of GelHFS compared to GelCD when implanted into a bone defect. Notably, more than 50 % of GelHFS hydrogel had degraded within two weeks of bone implantation, compared to only 40 % for GelCD. This rapid degradation did not occur *in vitro* or in subcutaneous implants, emphasizing the specificity of the bone environment in facilitating this process. This degradation property of GelHFS hydrogel facilitate endogenous cells infiltration and hence promoting new bone formation.

Our study has several limitations. We used proteomics to characterize the protein compositions of HFS, but more rigorous methods such as western blot and ELISA are needed to quantitatively verify the specific proteins presented in the bioinformatic analysis. Furthermore, as this initial study did not aim to specify the individual effects of each HFS compositions, the observed outcomes could be due to synergistic or additive effects of multiple proteins rather than a single factor. Identifying whether a specific protein or combination of proteins mediates the osteogenic effects of HFS requires further investigation.

5. Conclusion

This study demonstrates that incorporation of human fetal MSC secretome enhances the performance of gelatin-acrylated cyclodextrins hydrogels for bone tissue engineering applications. GelHFS hydrogel induces increased cell spreading, migration, and osteogenic differentiation of encapsulated MSCs. Moreover, GelHFS hydrogel creates a rejuvenating stem cell niche that supports the recruitment of endogenous progenitor cells and new bone formation, while accelerating degradation, leading to improved bone regeneration in an osteoporotic defect model. Ongoing proteomic analyses will identify specific HFS compositions contributing to its osteogenic effects. Overall, secretome-enhanced biomaterial scaffolds represent a promising approach for promoting osteoporotic bone repair.

Ethics approval and consent to participate

For the curent paper, the animal experiments are under Chinese University of Hong Kong Animal Experimentation Ethics Approval Ref No. 19-156-TBR and Ref No. 20- 136-MIS.

CRediT authorship contribution statement

Xiaoting Zhang: Writing – original draft, Methodology, Investigation, Data curation, Conceptualization. **Boguang Yang:** Methodology, Data curation, Conceptualization. **Lu Feng:** Validation, Methodology, Formal analysis. **Xiayi Xu:** Visualization, Methodology, Conceptualization. **Chenmin Wang:** Methodology, Data curation. **Yuk-wai Lee:** Supervision, Conceptualization. **Ming Wang:** Investigation. **Xuan Lu:** Investigation. **Ling Qin:** Resources, Funding acquisition. **Sien Lin:** Writing – review & editing, Supervision, Project administration, Methodology. **Liming Bian:** Resources, Project administration, Conceptualization. **Gang Li:** Writing – review & editing, Supervision, Funding acquisition, Conceptualization.

Declaration of competing interest

The authors have no conflicts of interest to disclose in relation to this article.

Acknowledgements

Health@InnoHK program launched by Innovation Technology Commission of the Hong Kong SAR, PR China.

Appendix A. Supplementary data

Supplementary data to this article can be found online at https://doi.org/10.1016/j.bioactmat.2024.07.036.

References

[1] J.-M. Féron, R. Mauprivez, Fracture repair: general aspects and influence of osteoporosis and anti-osteoporosis treatment, Injury 47 (2016) S10–S14.

[2] E. Yaacobi, D. Sanchez, H. Maniar, D.S. Horwitz, Surgical treatment of osteoporotic fractures: an update on the principles of management, Injury 48 (Suppl 7) (2017) S34–s40.

[3] C. von Rüden, P. Augat, Failure of fracture fixation in osteoporotic bone, Injury 47 (Suppl 2) (2016) S3–s10.

[4] B. Cortet, Bone repair in osteoporotic bone: postmenopausal and cortisone-induced osteoporos. Int. 22 (6) (2011) 2007–2010.

[5] W.H. Cheung, T. Miclau, S.K.-H. Chow, F.F. Yang, V. Alt, Fracture healing in osteoporotic bone, Injury 47 (2016) S21–S26.

[6] F. Shang, Y. Yu, S. Liu, L. Ming, Y. Zhang, Z. Zhou, J. Zhao, Y. Jin, Advancing application of mesenchymal stem cell-based bone tissue regeneration, Bioact. Mater. 6 (3) (2021) 666–683.

[7] V. Turinetto, E. Vitale, C. Giachino, Senescence in human mesenchymal stem cells: functional changes and implications in stem cell-based therapy, Int. J. Mol. Sci. 17 (7) (2016).

[8] D.G. Phinney, J. Galipeau, Manufacturing mesenchymal stromal cells for clinical applications: a survey of Good Manufacturing Practices at U.S. academic centers, Cytotherapy 21 (7) (2019) 782–792.

[9] B. Lukomska, L. Stanaszek, E. Zuba-Surma, P. Legosz, S. Sarzynska, K. Drela, Challenges and controversies in human mesenchymal stem cell therapy, Stem Cell. Int. 2019 (2019) 9628536.

[10] C.T. Laurencin, A. McClinton, Regenerative cell-based therapies: cutting edge, bleeding edge, and off the edge, Regen Eng Transl Med 6 (1) (2020) 78–89.

[11] G. Maguire, Stem cell therapy without the cells, Commun. Integr. Biol. 6 (6) (2013) e26631.

[12] E. Eggenhofer, F. Luk, M.H. Dahlke, M.J. Hoogduijn, The Life and fate of mesenchymal stem cells, Front. Immunol. 5 (2014).

[13] Y. Zhou, Y. Yamamoto, Z. Xiao, T. Ochiya, The immunomodulatory functions of mesenchymal stromal/stem cells mediated via paracrine activity, J. Clin. Med. 8 (7) (2019).

[14] Chapter 13 - stem cells and regenerative medicine, in: S.R. Goodman (Ed.), Goodman's Medical Cell Biology, fourth ed., Academic Press, 2021, pp. 361–380.

[15] S.H.M. Pang, J. D'Rozario, S. Mendonca, T. Bhuvan, N.L. Payne, D. Zheng, A. Hisana, G. Wallis, A. Barugahare, D. Powell, J. Rautela, N.D. Huntington, G. Dewson, D.C.S. Huang, D.H.D. Gray, T.S.P. Heng, Mesenchymal stromal cell apoptosis is required for their therapeutic function, Nat. Commun. 12 (1) (2021) 6495.

[16] B. Wang, W.Y. Lee, B. Huang, J.F. Zhang, T. Wu, X. Jiang, C.C. Wang, G. Li, Secretome of human fetal mesenchymal stem cell ameliorates replicative senescen, Stem Cell. Dev. 25 (22) (2016) 1755–1766.

[17] J. Xu, B. Wang, Y. Sun, T. Wu, Y. Liu, J. Zhang, W.Y. Lee, X. Pan, Y. Chai, G. Li, Human fetal mesenchymal stem cell secretome enhances bone consolidation in distraction osteogenesis, Stem Cell Res. Ther. 7 (1) (2016) 134.

[18] B. Wang, M. Pang, Y. Song, H. Wang, P. Qi, S. Bai, X. Lei, S. Wei, Z. Zong, S. Lin, X. Zhang, C. Cen, X. Wang, Y. Yang, Y. Li, Y. Wang, H. Xu, L. Huang, M. Tortorella, B. Cheng, T. Lee, D. Qin, G. Li, Human fetal mesenchymal stem cells secretome promotes scarless diabetic wound healing through heat-shock protein family, Bioengineering & Translational Medicine (2022).

[19] J. Xu, Q. Feng, S. Lin, W. Yuan, R. Li, J. Li, K. Wei, X. Chen, K. Zhang, Y. Yang, T. Wu, B. Wang, M. Zhu, R. Guo, G. Li, L. Bian, Injectable stem cell-laden supramolecular hydrogels enhance in situ osteochondral regeneration via the sustained co-delivery of hydrophilic and hydrophobic chondrogenic molecules, Biomaterials 210 (2019) 51–61.

[20] D.H.R. Kempen, L. Lu, A. Heijink, T.E. Hefferan, L.B. Creemers, A. Maran, M. J. Yaszemski, W.J.A. Dhert, Effect of local sequential VEGF and BMP-2 delivery on ectopic and orthotopic bone regeneration, Biomaterials 30 (14) (2009) 2816–2825.

[21] Q. Feng, J. Xu, K. Zhang, H. Yao, N. Zheng, L. Zheng, J. Wang, K. Wei, X. Xiao, L. Qin, L. Bian, Dynamic and cell-infiltrable hydrogels as injectable carrier of therapeutic cells and drugs for treating challenging bone defects, ACS Cent. Sci. 5 (3) (2019) 440–450.

[22] X. Xu, Q. Feng, X. Ma, Y. Deng, K. Zhang, H.S. Ooi, B. Yang, Z.Y. Zhang, B. Feng, L. Bian, Dynamic gelatin-based hydrogels promote the proliferation and self-renewal of embryonic stem cells in long-term 3D culture, Biomaterials 289 (2022) 121802.

[23] Q. Feng, K. Wei, S. Lin, Z. Xu, Y. Sun, P. Shi, G. Li, L. Bian, Mechanically resilient, injectable, and bioadhesive supramolecular gelatin hydrogels crosslinked by weak host-guest interactions assist cell infiltration and in situ tissue regeneration, Biomaterials 101 (2016) 217–228.

[24] W.Y.W. Lee, T. Zhang, C.P.Y. Lau, C.C. Wang, K.-M. Chan, G. Li, Immortalized human fetal bone marrow-derived mesenchymal stromal cell expressing suicide gene for anti-tumor therapy in vitro and in vivo, Cytotherapy 15 (12) (2013) 1484–1497.

[25] B. Yang, K. Wei, C. Loebel, K. Zhang, Q. Feng, R. Li, S.H.D. Wong, X. Xu, C. Lau, X. Chen, P. Zhao, C. Yin, J.A. Burdick, Y. Wang, L. Bian, Enhanced mechanosensing of cells in synthetic 3D matrix with controlled biophysical dynamics, Nat. Commun. 12 (1) (2021) 3514.

[26] X. Zhang, X. Wang, Y.-w. Lee, L. Feng, B. Wang, Q. Pan, X. Meng, H. Cao, L. Li, H. Wang, S. Bai, L. Kong, D.H.K. Chow, L. Qin, L. Cui, S. Lin, G. Li, Bioactive scaffold fabricated by 3D printing for enhancing osteoporotic bone regeneration, Bioengineering 9 (10) (2022) 525.

[27] Y. Moriya, M. Itoh, S. Okuda, A.C. Yoshizawa, M. Kanehisa, KAAS: an automatic genome annotation and pathway reconstruction server, Nucleic Acids Res. 35 (Web Server issue) (2007) W182–W185.

[28] Y. Li, Q. Pan, N. Zhang, B. Wang, Z. Yang, J.T. Ryaby, E.I. Waldorff, W.Y.-W. Lee, G. Li, A novel pulsed electromagnetic field promotes distraction osteogenesis via enhancing osteogenesis and angiogenesis in a rat model, Journal of Orthopaedic Translation 25 (2020) 87–95.

[29] L. Ye, J. Xu, J. Mi, X. He, Q. Pan, L. Zheng, H. Zu, Z. Chen, B. Dai, X. Li, Q. Pang, L. Zou, L. Zhou, L. Huang, W. Tong, G. Li, L. Qin, Biodegradable magnesium combined with distraction osteogenesis synergistically stimulates bone tissue regeneration via CGRP-FAK-VEGF signaling axis, Biomaterials 275 (2021) 120984.

[30] R.M. Wong, U. Thormann, M.H. Choy, Y.N. Chim, M.C. Li, J.Y. Wang, K.S. Leung, J. C. Cheng, V. Alt, S.K. Chow, W.H. Cheung, A metaphyseal fracture rat model for mechanistic studies of osteoporotic bone healing, Eur. Cell. Mater. 37 (2019) 420–430.

[31] H. Shin, B.D. Olsen, A. Khademhosseini, The mechanical properties and cytotoxicity of cell-laden double-network hydrogels based on photocrosslinkable gelatin and gellan gum biomacromolecules, Biomaterials 33 (11) (2012) 3143–3152.

[32] C. Harrell, C. Fellabaum, N. Jovicic, V. Djonov, N. Arsenijevic, V. Volarevic, Molecular mechanisms responsible for therapeutic potential of mesenchymal stem cell-derived secretome, Cells 8 (5) (2019) 467.

[33] S. Eleuteri, A. Fierabracci, Insights into the secretome of mesenchymal stem cells and its potential applications, Int. J. Mol. Sci. 20 (18) (2019).

[34] L. Lin, L. Du, The role of secreted factors in stem cells-mediated immune regulation, Cell. Immunol. 326 (2018) 24–32.

[35] J. Lotvall, A.F. Hill, F. Hochberg, E.I. Buzas, D. Di Vizio, C. Gardiner, Y.S. Gho, I. V. Kurochkin, S. Mathivanan, P. Quesenberry, S. Sahoo, H. Tahara, M.H. Wauben, K.W. Witwer, C. Thery, Minimal experimental requirements for definition of extracellular vesicles and their functions: a position statement from the International Society for Extracellular Vesicles, J. Extracell. Vesicles 3 (2014) 26913.

[36] P.D. Stahl, G. Raposo, Exosomes and extracellular vesicles: the path forward, Essays Biochem. 62 (2) (2018) 119–124.

[37] J.R. Ferreira, G.Q. Teixeira, S.G. Santos, M.A. Barbosa, G. Almeida-Porada, R. M. Goncalves, Mesenchymal stromal cell secretome: influencing therapeutic potential by cellular pre-conditioning, Front. Immunol. 9 (2018) 2837.

[38] M. Liang, W. Liu, Z. Peng, S. Lv, Y. Guan, G. An, Y. Zhang, T. Huang, Y. Wang, The therapeutic effect of secretome from human umbilical cord-derived mesenchymal stem cells in age-related osteoporosis, Artif. Cell Nanomed. Biotechnol. 47 (1) (2019) 1357–1366.

[39] Z. Zhao, G. Li, H. Ruan, K. Chen, Z. Cai, G. Lu, R. Li, L. Deng, M. Cai, W. Cui, Capturing magnesium ions via microfluidic hydrogel microspheres for promoting cancellous bone regeneration, ACS Nano 15 (8) (2021) 13041–13054.

[40] L. Li, M. Yu, Y. Li, Q. Li, H. Yang, M. Zheng, Y. Han, D. Lu, S. Lu, L. Gui, Synergistic anti-inflammatory and osteogenic n-HA/resveratrol/chitosan composite microspheres for osteoporotic bone regeneration, Bioact. Mater. 6 (5) (2021) 1255–1266.

[41] T. Wang, H. Ouyang, Y. Luo, J. Xue, E. Wang, L. Zhang, Z. Zhou, Z. Liu, X. Li, S. Tan, Y. Chen, L. Nan, W. Cao, Z. Li, F. Chen, L. Zheng, Rehabilitation exercise–driven symbiotic electrical stimulation system accelerating bone regeneration, Sci. Adv. 10 (1) (2024) eadi6799.

[42] S. Gronthos, P.J. Simmons, S.E. Graves, P.G. Robey, Integrin-mediated interactions between human bone marrow stromal precursor cells and the extracellular matrix, Bone 28 (2) (2001) 174–181.

[43] C.F. Lai, L. Chaudhary, A. Fausto, L.R. Halstead, D.S. Ory, L.V. Avioli, S.L. Cheng, Erk is essential for growth, differentiation, integrin expression, and cell function in human osteoblastic cells, J. Biol. Chem. 276 (17) (2001) 14443–14450.

[44] C. Ge, Q. Yang, G. Zhao, H. Yu, K.L. Kirkwood, R.T. Franceschi, Interactions between extracellular signal-regulated kinase 1/2 and P38 Map kinase pathways in the control of RUNX2 phosphorylation and transcriptional activity, J. Bone Miner. Res. 27 (3) (2012) 538–551.

[45] R.M. Salasznyk, R.F. Klees, A. Boskey, G.E. Plopper, Activation of FAK is necessary for the osteogenic differentiation of human mesenchymal stem cells on laminin-5, J. Cell. Biochem. 100 (2) (2007) 499–514.

[46] K.B.S. Paiva, J.M. Granjeiro, Matrix metalloproteinases in bone resorption, remodeling, and repair, Prog Mol Biol Transl Sci 148 (2017) 203–303.

[47] T. Nakatani, N.C. Partridge, Bone proteinases, Principles of Bone Biology (2020) 379–399.